ATLAS NOTE

ATLAS-CONF-2013-002

January 11, 2013

# Jet energy measurement and systematic uncertainties using tracks for jets and for b-quark jets produced in proton-proton collisions at $\sqrt{s} = 7$ TeV in the ATLAS detector

The ATLAS Collaboration

**Abstract**

Studies of the jet energy scale are performed in an inclusive QCD jet sample with and without *b*-tagging and in a sample of top quark pairs, using in situ methods and Monte Carlo simulated samples. The correlation between the calorimeter jet transverse momentum ($p_{\mathrm{T}}$) and the total transverse momentum of tracks pointing to the jet is used to study the calorimeter jet energy scale. Agreement in this correlation is found between Monte Carlo simulation and data for jets tagged as *b*-jets as well as for samples enriched in light jets within systematic uncertainties of about 4%. Many systematic effects cancel in the ratio of the $p_{\mathrm{T}}$ measurement for *b*-tagged jets to the measurement for light jets, resulting in a reduced systematic uncertainty of about 2% on the ratio between the *b*-jet and light-jet energy scales. The $p_{\mathrm{T}}$ imbalance in the dijet system is used to validate the modeling of the neutrino energy carried by *b*-jets decaying semileptonically to a muon and a neutrino. Agreement between data and Monte Carlo simulation is found, within the 2% uncertainty of the method.

# 1 Introduction

Jets produced in proton-proton collisions at the Large Hadron Collider (LHC) at CERN are key ingredients for many physics measurements and for searches for new physics. Systematic effects affecting the jet energy measurement are generally among the dominant sources of experimental uncertainty for many of these analyses, and in particular the uncertainty on the jet energy scale associated with jets initiated by a $b$-quark ($b$-jets) plays an important role in precision measurements such as that of the top quark mass [1]. The uncertainty on the energy scale of $b$-jets also enters the $b$-tagging calibration analyses, further contributing to the systematic uncertainties for measurements of final states with $b$-jets [2, 3].

In this note, as in Ref. [4], the measurement of the jet energy is studied using Monte Carlo simulations and in-situ techniques, using the ratio of the transverse momentum ($p_{\mathrm{T}}$) of the vector sum of all tracks in the jet cone to the calorimeter jet $p_{\mathrm{T}}$:

$$r_{\mathrm{trk}} = \frac{\sum \vec{p}_{\mathrm{T}}^{\,\mathrm{track}}}{p_{\mathrm{T}}^{\mathrm{jet}}}. \quad (1)$$

These studies assess the jet energy measurement in the calorimeter in light-jet enriched samples as well as for $b$-jet enriched samples in an inclusive jet sample and in an event sample where a top-quark pair is produced ($t\bar{t}$). The uncertainty on the $b$-jet energy measurement is thus evaluated over a wide range of $p_{\mathrm{T}}$ and under different background conditions. Furthermore, the $p_{\mathrm{T}}$ imbalance in a dijet system is used to validate the description of the kinematics of the neutrino coming from $b$-quarks decaying semileptonically in the Monte Carlo simulation.

In the following we will refer to $b$-tagged jets as jets containing $b$-hadrons ($b$-jets) that are identified by means of $b$-tagging techniques. The notation inclusive jets will be used to denote a mixture of light-quark-, $b$- and gluon-initiated jets.

The analyses presented here are based on a dataset corresponding to an integrated luminosity of about 4.7 fb$^{-1}$ of proton-proton collisions with a center-of-mass energy of $\sqrt{s} = 7$ TeV collected in the 2011 running period by the ATLAS detector. A description of the detector can be found elsewhere [5].

# 2 Object reconstruction and selection

## 2.1 Jet reconstruction and selection

Jets are reconstructed using the anti-$k_t$ jet algorithm with a distance parameter $R = 0.4$ or $R = 0.6$ [6]. ATLAS has developed several jet calibration schemes [7] with different levels of complexity. Each calibration scheme starts from the measured calorimeter energy at the electromagnetic (EM) energy scale [8–16], which correctly measures the energy deposited by electromagnetic showers. The local cluster weighting (LCW) calibration method first calibrates topologically connected calorimeter cells according to their properties. The final jet energy calibration is derived as a simple correction relating the calorimeter response to the true jet energy. It can be applied to EM scale jets, with the resulting calibrated jets referred to as EM+JES, or to LCW calibrated jets, with the resulting jets referred to as LCW+JES jets. In this document, jets calibrated with the EM+JES calibration and reconstructed with $R = 0.4$ are used for most studies, since the calibration of the $b$-tagging algorithms has been performed only for these jets. For studies in the inclusive jet sample, for which $b$-tagging is not needed, jets calibrated with the LCW+JES calibration and jets reconstructed with $R = 0.6$ are also studied. Jets with a calibrated transverse momentum $p_{\mathrm{T}}^{\mathrm{jet}} > 20$ GeV and a pseudorapidity $|\eta| < 2.5$[1] are used in this study.

[1] ATLAS uses a right-handed coordinate system with its origin at the nominal interaction point (IP) in the center of the detector and the $z$-axis along the beam pipe. The $x$-axis points from the IP to the centre of the LHC ring, and the $y$ axis points upward. Cylindrical coordinates $(r, \phi)$ are used in the transverse plane, $\phi$ being the azimuthal angle around the beam pipe. The pseudorapidity is defined in terms of the polar angle $\theta$ as $\eta = -\ln\tan(\theta/2)$.

Two aspects of the jet energy scale are studied separately: the response to particles absorbed in the calorimeter and the detector response to all produced particles including muons and neutrinos. The former is characterized by the calorimeter response $\mathcal{R}^{\text{calo}} = p_{\text{T}}^{\text{jet}}/p_{\text{T}}^{\text{truth}}$, where $p_{\text{T}}^{\text{truth}}$ is the $p_{\text{T}}$ of a matched jet built from final state particles with a lifetime longer than 10 ps, except for muons and neutrinos. The latter is characterized by the all-particle response $\mathcal{R}^{\text{all}} = p_{\text{T}}^{\text{jet}+\mu}/p_{\text{T}}^{\text{truth,all}}$, where $p_{\text{T}}^{\text{jet}+\mu}$ includes selected reconstructed muons inside the jet and $p_{\text{T}}^{\text{truth,all}}$ is the $p_{\text{T}}$ of a matched jet built of final state particles with a lifetime longer than 10 ps, including muons and neutrinos.

The jet energy scale of $b$-tagged jets in the dijet sample is studied using different $b$-tagging algorithms. For each algorithm, different operating points resulting in different efficiencies and purities are studied, as detailed in Section 3. In the Monte Carlo simulation, the flavor of jets is determined as described in Ref. [2], by the presence of a heavy-flavor quark matched geometrically to the reconstructed jet ($\Delta R = \sqrt{(\eta^{\text{jet}} - \eta^{\text{quark}})^2 + (\phi^{\text{jet}} - \phi^{\text{quark}})^2} < 0.3$).

In the $t\bar{t}$ sample $b$-tagged jets are selected by means of the MV1 tagger [17]. The MV1 tagger uses the results from three $b$-tagging algorithms exploiting secondary-vertex and track-impact-parameter information, which are input to a neural network to derive a likelihood discriminant to select $b$-jets. In this analysis, a jet is experimentally identified as a $b$-jet if the MV1-tagger weight ($w_{\text{MV1}}$) exceeds a threshold value of 0.6. This corresponds to 70% per-jet efficiency for selecting $b$-jets from $t\bar{t}$ decays, and a per-jet rejection factor for light-quark jets of about 130. To adjust the Monte Carlo simulation to the $b$-tagging performance in data, a dedicated $b$-tagging efficiency correction [17] is applied to the simulation and the related systematic uncertainties are evaluated.

The influence of nearby jets on the measurements has been studied by applying an isolation requirement which rejects jets that are separated from the nearest other jet by a distance $\Delta R < 2R$. The influence of this requirement has been found to be negligible in the analyses presented, so the requirement is omitted in the results shown.

To study the impact of energy induced by particles produced in multiple proton-proton interactions, the jet vertex fraction (JVF) algorithm is used to quantify the amount of energy coming from these 'pile-up' interactions. After associating tracks to jets ($\Delta R(\text{jet}, \text{track}) < 0.4$), the JVF is defined as the scalar summed transverse momentum of associated tracks from the primary vertex divided by the summed transverse momentum of associated tracks from all vertices.

## 2.2 Track selection

Tracks are associated with jets by requiring that the opening angle between the track and the jet direction $\Delta R(\text{jet}, \text{track}) < 0.4$. Track parameters are evaluated at the distance of closest approach to the primary hard-scattering vertex, defined as that with the highest sum of track $p_{\text{T}}^2$. Tracks are required to meet the following selection criteria to ensure good tracking quality, and to minimize the contributions from photon conversions and from tracks not arising from the primary hard-scattering vertex:

- track transverse momentum $p_{\text{T}}^{\text{track}} > 1$ GeV,
- number of pixel hits ≥1, number of hits in the silicon strip tracker ≥6,
- track impact parameter with respect to the hard-scattering vertex:

$$|d_0| < 1.5 \text{ mm and } |z_0 \cdot \sin(\theta)| < 1.5 \text{ mm},$$

where $d_0$ refers to the distance in the transverse plane and $z_0$ to the distance along the beam pipe.

# 3 Event selection

The data sample has been collected with all ATLAS sub-detectors operational. It corresponds to a total integrated luminosity of about 4.7 fb$^{-1}$ of proton-proton collisions at $\sqrt{s} = 7$ TeV, collected between February and October of 2011 with a bunch spacing of 50 ns. The average number of interactions per bunch crossing was 6 in the initial, low-luminosity, part of the run, and 11 in the final, high-luminosity, part of the run, ranging overall from 3 to 17. Events have been collected by means of single-jet and single-lepton triggers. A primary vertex reconstructed from at least five tracks, which is consistent with the position and transverse size of the beam, is required. Analysis-specific selections are described below.

## 3.1 Jet sample selection

Four complementary event selections are used for studies in the dijet sample:

1. An inclusive selection is used to study the energy calibration in the QCD jet sample, and uses 11 single-jet triggers to cover the full $p_{\mathrm{T}}$ range, to cope with the reduced data rate allowed for lower $p_{\mathrm{T}}$ triggers.

2. Two $b$-tagged jet selections are used to study the energy calibration of $b$-jets,

   (a) an inclusive $b$-tagged sample is selected using five different single-jet triggers, since the range of $p_{\mathrm{T}}$ for $b$-jet studies is limited by the low trigger rates at low $p_{\mathrm{T}}$ and by the measurements of $b$-tagging efficiencies at high $p_{\mathrm{T}}$,

   (b) a semileptonic $b$-tagged sample is selected using a single muon-jet trigger [2], requiring a muon candidate inside a jet, which is less heavily prescaled, increasing the size of the sample collected with respect to a sample collected with a single jet trigger.

3. A dijet selection is used to study the impact of semileptonic decays into muons and neutrinos.

Only one trigger is used to collect events in one specific $p_{\mathrm{T}}$ bin. This procedure has been verified to be compatible within statistical uncertainties with a procedure that combines all jet triggers in each bin weighting events according to the integrated luminosity collected by the trigger that allowed the event to be recorded.

The measurement in the dijet sample is performed as a function of the average $p_{\mathrm{T}}$ ($p_{\mathrm{T}}^{\mathrm{avg}}$) of the two leading jets, including the muon candidate if one is reconstructed inside the jet. The estimated muon energy loss in the calorimeter active layers is subtracted to avoid double counting. The measurement in the inclusive samples is performed as a function of $p_{\mathrm{T}}^{\mathrm{jet}}$. The dijet event selection further requires:

- at least two jets with $p_{\mathrm{T}}^{\mathrm{jet}} > 20$ GeV, $|\eta| < 1.2$ (to ensure that the $p_{\mathrm{T}}$ balance is not affected by instrumental effects) and $|\mathrm{JVF}| > 0.75$,
- the two leading jets in $p_{\mathrm{T}}$ $b$-tagged with the MV1 algorithm ($w_{\mathrm{MV1}} > 0.6$),
- at least one of the jets with a muon candidate of $p_{\mathrm{T}} > 4$ GeV within $\Delta R = 0.4$ passing the selection described in Ref. [2],
- no third leading jet with $|\mathrm{JVF}| > 0.6$ and $p_{\mathrm{T}}^{\mathrm{jet}} > \max(12\ \mathrm{GeV}, 0.25 \cdot p_{\mathrm{T}}^{\mathrm{avg}})$,
- $\Delta\phi_{jj} > 2.5$.

The selection on the inclusive samples requires at least one jet with $p_{\mathrm{T}}^{\mathrm{jet}} > 25$ GeV and $|\eta| < 2.5$, and the |JVF| > 0.75 cut. The muon selection is unchanged and different *b*-tagging algorithms and operating points are studied, since the neutrino energy is expected to be largely independent of the tagging algorithm, but the jet energy scale is not.

The *b*-jet purity of these samples is measured in the Monte Carlo simulation to vary from 50% to 70% for the inclusive selection, 60% to 80% for the semileptonic selection, and above 80% for the dijet selection for the operating points studied. Observations at high $p_{\mathrm{T}}$ ($p_{\mathrm{T}} \gtrsim 200$ GeV) suggest that the purity might be underestimated by as much as about 10% [18]. Uncertainties on the efficiency of the tagging algorithm to identify *b*-jets and *c*-jets can also impact these purity estimates by up to about 10% [2]. Despite these systematic effects, the purity of these samples remains sufficiently large for the validation purposes of this study.

### 3.2 Top-quark pair sample selection

Top quark pair events where one of the *W*-bosons produced by the top quark decays to an electron or a muon are selected by requiring (see Ref. [1] for further details):

- a single lepton trigger,
- exactly one electron ($e$) with transverse energy above 25 GeV, within pseudorapidity range of $|\eta|$ less than 2.47, and outside the region of transition between the barrel and the endcap calorimeters, $1.37 \leq |\eta| < 1.52$; or exactly one muon ($\mu$) with transverse momentum above 20 GeV, within $|\eta| < 2.5$. The reconstructed charged lepton has to match the trigger object corresponding to the required triggers that passed,
- for the $t\bar{t} \rightarrow$ e+jets channel the transverse *W*-boson mass, $m_T(W)$, reconstructed from the electron and the missing transverse momentum, $E_{\mathrm{T}}^{\mathrm{miss}}$ [19], should be $m_T(W) > 25$ GeV, and $E_{\mathrm{T}}^{\mathrm{miss}} > 35$ GeV; alternatively, for the $t\bar{t} \rightarrow \mu$+jets channel, $E_{\mathrm{T}}^{\mathrm{miss}} > 25$ GeV and $E_{\mathrm{T}}^{\mathrm{miss}} + m_T(W) > 60$ GeV are required,
- at least four jets with $p_{\mathrm{T}}^{\mathrm{jet}} > 25$ GeV, |JVF| > 0.75 and $|\eta| < 2.5$ are required. Among these, at least two jets should be *b*-tagged using the MV1 *b*-tagging algorithm ($w_{\mathrm{MV1}} > 0.6$).

After this selection the background contamination in the $t\bar{t}$ sample is expected to be of order 10% and to mainly consist of events from $W/Z$+jets and single top-quark production. The contribution from QCD multijet background after the requirement of two b-tagged jets is expected to be about 4%. The background contamination in the selected data sample has no sizable impact in the studies performed. The change in the results when including the background in the analysis is treated as a systematic uncertainty.

## 4 Monte Carlo simulation samples

Simulated event samples are generated for comparisons with data and for the determination of the systematic uncertainty based on variations in the Monte Carlo generator settings. Additional minimum bias pile-up events are generated with either Pythia6 [20] with the ATLAS MC11 AUET2B tune [21] using the CTEQ6L1 parton distribution function (PDF) [22] or Pythia8 [23] with the 4C tune, and superimposed on the hard-scattering event. The impact of this choice on the analyses is negligible. The number of pile-up events is chosen to match the conditions found in the data. The events are passed through the ATLAS detector simulation [24] and are reconstructed using the same software as for the data.

### 4.1 Dijet Monte Carlo simulation samples

The baseline (nominal) Monte Carlo sample used to derive the jet energy scale is a sample of inclusive jets at high transverse momentum. It is generated with the PYTHIA 6 [20] event generator with the AUET2B tune [21]. The modified leading-order PDF set MRST LO* [25] is used. This sample is referred to alternatively as PYTHIA MC11.

Systematic uncertainties are studied using variations of the Monte Carlo simulation as in Ref. [4]: the fragmentation and hadronization modeling uncertainty is estimated by comparing the Monte Carlo generators HERWIG++ [26] and PYTHIA. The soft physics modeling uncertainty is evaluated by comparing the PYTHIA AUET2B to the PYTHIA PERUGIA2011 tune [27]. The modeling uncertainty related to the detector material in front of the calorimeters is studied using Monte Carlo events reconstructed with a modified ATLAS geometry containing additional material in the tracking volume and in front of the calorimeters. Finally, to assess the impact of the *b*-quark fragmentation settings, the nominal parameters of the PYTHIA fragmentation function are replaced by the values from a recent tune using the Professor framework [28]. In addition, the nominal fragmentation function is replaced by the modified Bowler-Lund fragmentation function [29].

### 4.2 Top-quark pair Monte Carlo simulation samples

The nominal sample of $t\bar{t}$ events used in top-quark analyses in ATLAS is generated using the MC@NLO [30] generator v4.01 with the CT10 [31] parton distribution function. The MC@NLO program contains the matrix element for top pair production calculated at next-to-leading order interfaced to parton showers. The parton shower and the underlying event were added using the HERWIG v6.520 [32] and JIMMY 4.31 [33] programs with the CT10 PDF [31] and the ATLAS AUET2 tune [34].

A number of samples using alternative Monte Carlo generators or different generator parameter configurations are used to estimate systematic uncertainties. Additional $t\bar{t}$ samples are simulated using the POWHEG [35] generator interfaced with PYTHIA, as well as HERWIG and JIMMY. The POWHEG software contains a different implementation of the next-to-leading order matrix element calculation and interface to parton showers. These samples enable the comparisons of two different parton-shower, hadronization and fragmentation models and also a comparison of the POWHEG and MC@NLO implementations of the NLO matrix element calculations. Differences in the *b*-hadron decay tables between PYTHIA and HERWIG are also large enough to provide a conservative uncertainty on the effects of the decay model. Unlike in most top-quark analyses in ATLAS, in the studies presented here, samples generated with POWHEG+PYTHIA are used as the default, so that direct comparisons with the analysis in the inclusive jet sample are possible. Additional results obtained by using MC@NLO+HERWIG+JIMMY as the default sample for the comparison with the data are reported in Appendix A.

In addition, samples with more and less parton shower activity generated with the leading order generator ACERMC [36] interfaced to PYTHIA, with the MRST LO** PDF set [37], are used to estimate the model dependence of the event selection. In these samples the initial and final state radiation (ISR/FSR) parameters are set to a range of values not excluded by the current experimental data, as detailed in Ref. [1, 38].

## 5 Monte Carlo-based systematic uncertainties on the calorimeter *b*-jet energy scale

The uncertainties on the *b*-jet transverse momentum measurement are studied using systematic Monte Carlo variations. The *b*-jet can be either reconstructed using a calibration with respect to all stable particles (to study the all-particle energy scale) or excluding muons and neutrinos (to study the calorimeter

energy scale), as described in Section 2.1. The former definition is currently most relevant for *b*-tagging calibration analyses [2], and further discussed in Section 7.

The uncertainty in the calorimeter response to *b*-jets can be estimated using a combination of different Monte Carlo simulations as reported in Ref. [4]. Figure 1a shows the calorimeter response to *b*-jets for various Monte Carlo simulations.

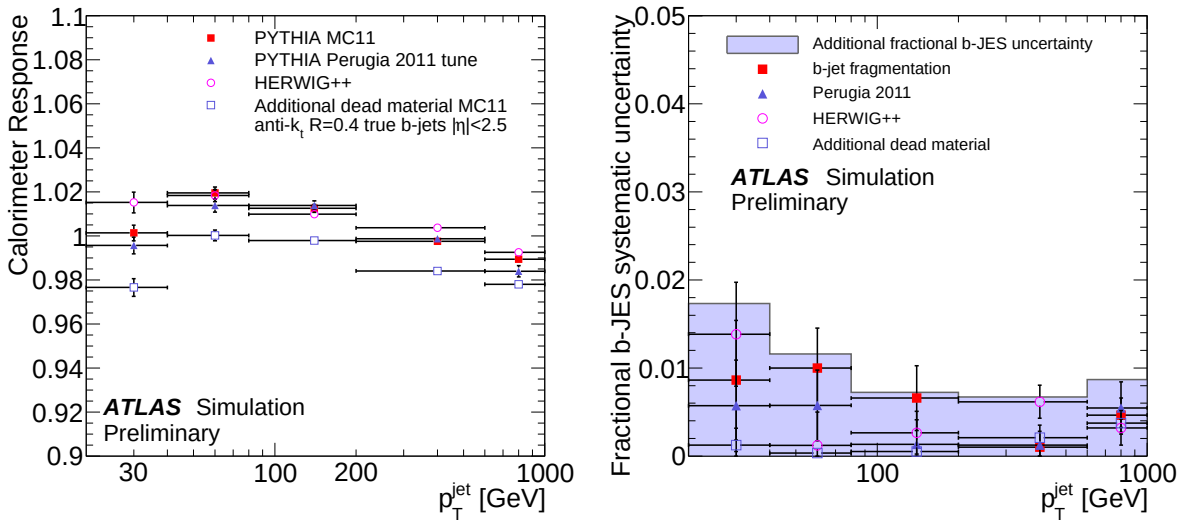


(a) Response (b) Uncertainty

Figure 1: Average response of *b*-jets in some of the different samples used to calculate the *b*-jet energy scale systematic uncertainties (a) and resulting uncertainties in the ratio of the *b*-jet response to the response of jets in an inclusive sample (b). Results are shown for *b*-jets built with the anti-$k_t$ algorithm with resolution parameter $R = 0.4$.

The corresponding systematic uncertainties associated with the *b*-jet energy measurement are shown in Figure 1b. These uncertainties need to be considered in addition to those established for an inclusive jet sample in Ref. [39], since *b*-jet specific effects were not treated in that analysis. These uncertainties can be applied to any sample of *b*-jets, whether a specific analysis uses tagging or not, and are of a size comparable to the uncertainties in the *in situ* measurements presented later in this document.

Two key changes have happened in this analysis with respect to what was reported in Ref. [4]. The dead material uncertainty (which is large in Figure 1a, but does not contribute significantly to the systematic uncertainty reported in Figure 1b) is calculated as the *additional* change in the response expected from dead material effects for a *b*-jet sample with respect to an inclusive sample (or a pure light-quark sample for comparable results). This is possible in 2011 because in-situ jet energy scale corrections and uncertainties exist, already accounting for a potential mismodeling of the dead material in the Monte Carlo simulation. The uncertainty component derived from the propagation of single-particle uncertainties to jets (single-particle uncertainty) is also removed, while it contributed 0.5% in 2010. This result relies again on the in-situ studies, since differences in the calorimeter response between data and Monte Carlo simulation are already taken into account in those studies. Residual effects that could give rise to an additional systematic uncertainty component for *b*-jets have been constrained using a single-particle study and are shown in Ref. [39].

# 6 Calorimeter jet energy measurement validation using tracks

The calorimeter jet energy scale can be probed by comparing the measured jet energy to that of a well calibrated reference object. Charged particle tracks, which are both well measured and independent of the calorimeter and are associated with jets as described in Section 2.2, are used here. The mean value of $r_{\mathrm{trk}}$, defined in Eq. 1, is primarily sensitive to the particle composition of the jet and so should be well described by any well-tuned event generator. In computing $\langle r_{\mathrm{trk}} \rangle$ it is important to truncate the $r_{\mathrm{trk}}$ distribution (here truncated at $r_{\mathrm{trk}} = 3$) to avoid the effect produced by fake tracks with unphysically large $p_{\mathrm{T}}$.

To verify the description in the Monte Carlo simulation of the calorimeter energy measurement, the double ratio of the charged-to-total momentum obtained in data to that obtained in Monte Carlo simulation is studied:

$$R_{\mathrm{r_{trk}}} \equiv \frac{[\langle r_{\mathrm{trk}} \rangle]_{\mathrm{Data}}}{[\langle r_{\mathrm{trk}} \rangle]_{\mathrm{MC}}}. \tag{2}$$

The ratio is evaluated for inclusive jets, $b$-tagged jets and $b$-tagged jets with a reconstructed muon inside (in the dijet sample only). In the following they will be referred to as $R_{\mathrm{r_{trk},inclusive}}$, $R_{\mathrm{r_{trk},b\text{-jet}}}$ and $R^{\mu\nu}_{r_{\mathrm{trk}},b\text{-jet}}$. The calorimeter response to $b$-tagged jets relative to inclusive jets, $R'$, is defined as

$$R' \equiv \frac{R_{r_{\mathrm{trk}},b\text{-jet}}}{R_{\mathrm{r_{trk},inclusive}}}. \tag{3}$$

This ratio is used to test the relative systematic uncertainty between $b$-tagged and inclusive jets. In the $t\bar{t}$ sample, where the fraction of $b$-jets is large ($\approx 50\%$), the light jets (non $b$-tagged) component is used in the denominator instead of the inclusive one. It is mainly comprised of jets from the $W$-boson decay but also to a minor extent of gluon-jets from initial and final state radiation. As a consequence, when comparing the results obtained by the $t\bar{t}$ and the dijet analyses, the difference in terms of jet flavor components entering the calculation of $R_{\mathrm{r_{trk},inclusive}}$ should be taken into consideration.

## 6.1 Systematic uncertainties

Systematic uncertainties in the $r_{\mathrm{trk}}$ measurement arise from the modeling of the jet (and $b$-jet) fragmentation, $b$-tagging calibration, jet resolution and tracking efficiency. In addition, for high-$p_{\mathrm{T}}$ jets ($p_{\mathrm{T}} > 500$ GeV) an efficiency loss in the tracking in the jet core has been observed in Monte Carlo simulation, and a systematic uncertainty is added to account for potential mismodeling of this effect. These uncertainties are assumed to be uncorrelated. The resulting fractional systematic uncertainties on $r_{\mathrm{trk}}$ and $R'$ are shown on Figure 2b, d, f and Figure 3b, d, f and are determined as follows:

1. **MC generator and tunes:** These systematic uncertainties capture the effects of differences in $p_{\mathrm{T}}^{\mathrm{trk}}$ caused by different fragmentation models. Differences in the calorimeter response, caused by the different particle spectra, can also impact the $r_{\mathrm{trk}}$ measurement in certain Monte Carlo simulations and should not be part of the uncertainty, since such shifts are measurable in the data. The $r_{\mathrm{trk}}$ distribution is, thus, calculated from the various samples described in Section 4 using $p_{\mathrm{T}}^{\mathrm{truth}}$ in the denominator, even though only small differences have been observed when including calorimeter effects, i.e. using $p_{\mathrm{T}}^{\mathrm{calo}}$ in most samples. In the $t\bar{t}$ analysis, differences between MC@NLO and POWHEG+HERWIG are considered as process or generator systematic uncertainties. Fragmentation and decay systematic uncertainties are evaluated conservatively taking the difference between PYTHIA and HERWIG. In the dijet analysis, differences between PYTHIA and HERWIG++ set the systematic uncertainties from uncertainties in the decay models. The updated fragmentation tune in

HERWIG++ prevents this comparison from being a conservative measure of the $b$-jet fragmentation systematic uncertainties. These are evaluated using comparisons to the Bowler-Lund and Professor tunes described before.

2. **$b$-tagging calibration:** The scale factors that correct the $b$-tagging efficiencies in Monte Carlo simulation to match the measured values are varied within their total uncertainty.

3. **Material description:** The knowledge of the tracking efficiency modeling in Monte Carlo simulation was evaluated in detail in Ref. [40]. The systematic uncertainty on the tracking efficiency for isolated tracks increases from 2% ($|\eta^{\text{track}}| < 1.3$) to 7% ($2.3 \leq |\eta^{\text{track}}| < 2.5$) for tracks with $p_{\text{T}} > 500$ MeV. The resulting effect on $r_{\text{trk}}$ is about 3% for $0 \leq |\eta| < 2.1$ and about 4% for $2.1 \leq |\eta| < 2.5$.

4. **Tracking in jet core:** High track densities in the jet core influence the tracking efficiency due to shared hits between tracks, fake tracks and lost tracks. The number of shared hits is well-described in the Monte Carlo simulation. The $p_{\text{T}}$ carried by fake tracks is negligible. A relative systematic uncertainty of 50% on the loss of efficiency obtained in the simulation is assigned to account for potential mismodeling of this effect.

5. **Jet resolution:** The jet energy resolution in the Monte Carlo simulation is degraded by about 10%.

6. **Background contamination:** for the $t\bar{t}$ sample the analysis is repeated including the expected background contamination (except the QCD multijet contribution) and the full difference is taken as an estimate of the systematic uncertainty.

The dominant contributions to the systematic uncertainty in the $t\bar{t}$ analysis are due to variations in the detector material and fragmentation/decay models. In the dijet sample, the material, fragmentation and decay uncertainties also dominate the systematic uncertainties, except at $p_{\text{T}} \gtrsim 500$ GeV where the uncertainty caused by the loss of efficiency in the jet core dominates. In Figure 3, the contributions to the total systematic uncertainty due to the jet resolution, $b$-tagging calibration, background contamination and due to the modeling of the initial and final state radiation are labeled as "other" systematic uncertainties.

For $R'$, the tracking components (the material description, impacting the tracking efficiency) of the systematic uncertainty entering both the numerator and denominator are correlated and thus approximately cancel. A similar consideration holds for the jet energy resolution. The most significant systematic uncertainties on $R'$ are due to the choice of the Monte Carlo generator and the fragmentation and decay models.

## 6.2 Results

Figure 2a,c shows the ratio of the average of the $r_{\text{trk}}$ distribution in data and Monte Carlo simulation for jets in the inclusive jet sample sample with $|\eta| < 1.2$. Figure 2b,d shows the different components of the associated systematic uncertainty. The study in the sample without $b$-tagging covers up to approximately 2 TeV, and provides a cross check across almost the full range of calibrated $p_{\text{T}}$ studied in situ through the analyses used to establish the systematic uncertainty on the jet energy scale in ATLAS [39]. No $p_{\text{T}}$ dependence is observed and agreement is found between data and Monte Carlo simulation within systematic uncertainties. Similar results have been found in higher $|\eta|$ regions.

Agreement of the Monte Carlo simulation with the data for the $r_{\text{trk}}$ measurements is found within systematic uncertainties across all $p_{\text{T}}$ for inclusive jets and for $p_{\text{T}}^{\text{jet}} < 400$ GeV for $b$-tagged jets. The relative response $R'$ between $b$-tagged and inclusive jets is shown in Figure 2e and the uncertainty band corresponds to the relative $b$-jet energy scale uncertainty with respect to the inclusive jet sample. Figure 2f shows the different components of the associated systematic uncertainty. A difference between data and

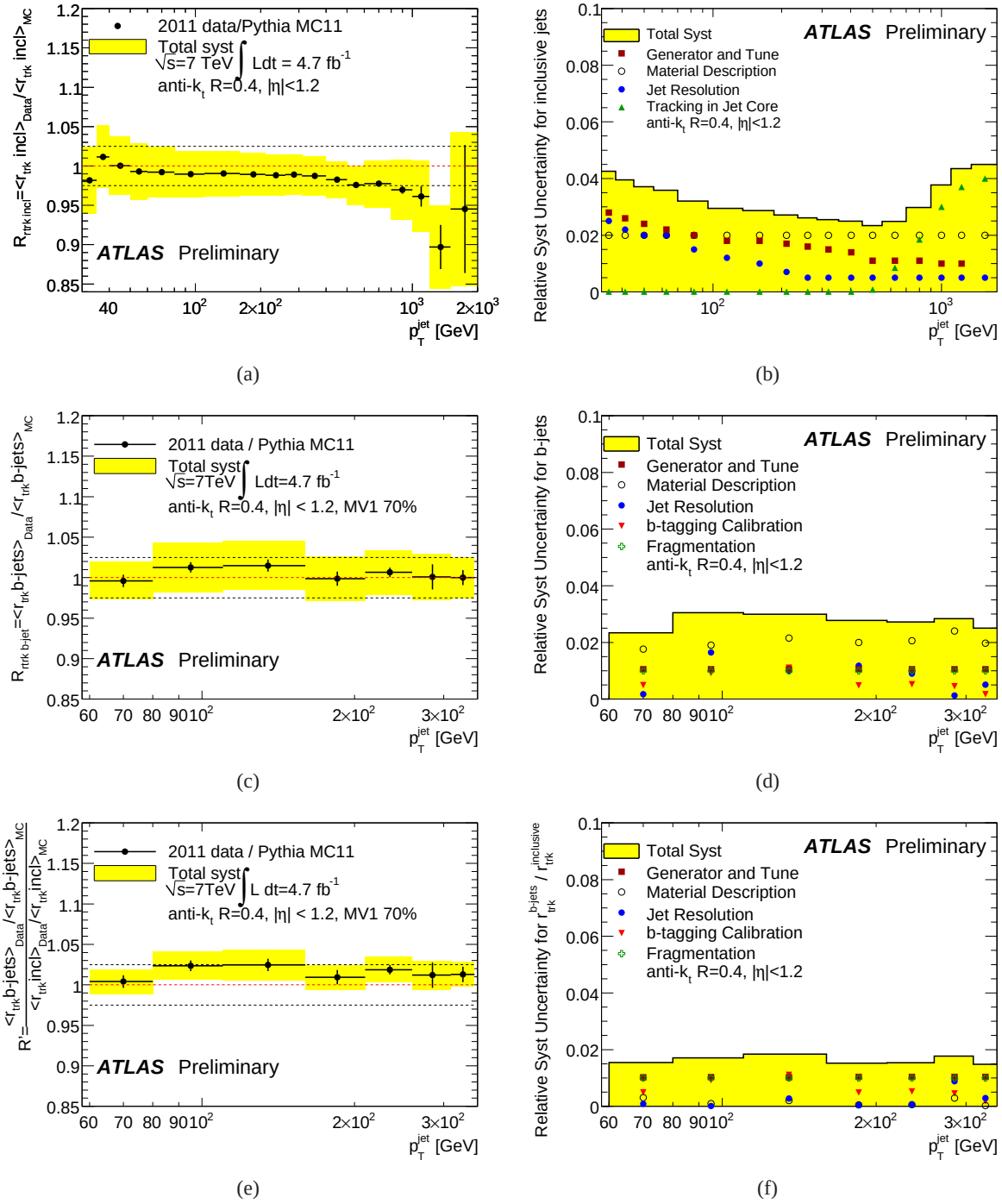


Figure 2: Ratio of the average $r_{\mathrm{trk}}$ in data and Monte Carlo simulation for inclusive jets (a), tagged $b$-jets (c), and ratio of $R_{r_{\mathrm{trk}}}$ between the $b$-jet and the inclusive sample (e). The contributions of the systematic uncertainties to the total uncertainty in the different measurements are shown in b, d, f. Jets with $|\eta| < 1.2$ were used for these figures.

Monte Carlo simulation is found but almost covered by the systematic uncertainties. This difference is partially caused by the overall 1% shift found in the inclusive sample. Similar results have been found in the sample of $b$-jets decaying to muons selected in the dijet sample, with a larger difference between data and Monte Carlo simulation of up to 4% in the lowest $p_{\mathrm{T}}$ bin probed. However, the uncertainties in the modeling are also somewhat larger, limiting the constraints on the jet energy scale of these jets to approximately 3%.

The corresponding results from the same study performed in the $t\bar{t}$ sample are shown in Figure 3. The results in this sample are consistent with those obtained in the dijet sample, except for the better agreement between data and Monte Carlo simulation in the light-jet sample, which also leads to better agreement in the $b$-jet to light-jet sample results. The systematic uncertainties are also comparable, despite the different methods used in their evaluation. The uncertainty in the in-situ technique used to assess the $b$-jet energy scale is estimated to be approximately 2.5% and 3% in the ranges $|\eta| < 1.2$ and $1.2 \leq |\eta| < 2.5$, respectively, for jets with $p_{\mathrm{T}}^{\mathrm{jet}} < 400$ GeV from these studies.

## 7 Semileptonic correction and associated uncertainties

The study of the all-particle response of $b$-jets, $\mathcal{R}^{\mathrm{all}}$, i.e. the energy scale calculated with respect to jets built using all stable particles, is also necessary for many analyses, given that about 40% of $b$-jets decay semileptonically, thus having a non-negligible amount of their energy carried by neutrinos. In particular, the study of the $b$-tagging efficiency in a sample of $b$-jets decaying semileptonically to muons [2] requires a correction that maps the all-particle jet energy scale of that sample to that of an inclusive sample of $b$-jets. This correction and its systematic uncertainties are estimated in this section. The correction also has applications beyond the $b$-tagging calibration since it can also be used to improve the reconstruction of $b$-jets identified as semileptonic. The study of the all-particle energy scale in this section is performed independently of the study of the calorimeter energy scale, even though the two are not straightforward to decouple in in-situ studies.

Figure 4a shows the all-particle response for an inclusive jet sample, a sample of $b$-jets tagged with the MV1 algorithm and a sample of $b$-jets containing a muon from a semileptonic $b$ decay. The semileptonic $b$-jets sample is selected using hadron-level information, and no $b$-tagging is imposed. However, the muon is required to pass kinematic and quality cuts detailed in Ref. [2]. The effect of neutrinos is clearly visible in both the tagged $b$-jet sample and more significantly in the semileptonic $b$-jets sample. The rise at low $p_{\mathrm{T}}$ in the semileptonic sample arises from biases created by the muon kinematic cuts.

The response of semileptonically decaying $b$-jets is corrected to that of an inclusive $b$-tagged jet sample. The correction is constructed using techniques similar to those used in the EM+JES calibration [4], introduced in Section 2.1. This correction is shown in Figure 4b, as a function of calibrated jet $p_{\mathrm{T}}$ for fixed muon $p_{\mathrm{T}}$ and jets with $|\eta| < 0.8$. The correction is not explicitly dependent on $p_{\mathrm{T}}^{\mu}$ even though it enters in the calculation of the reconstructed jet $p_{\mathrm{T}}$ used to compute the correction.

Systematic uncertainties in this correction need to account for our knowledge of $b$-jet fragmentation and decay, as well as the effect of the muon spectrum and muon reconstruction. These uncertainties have been studied in Ref. [2]. Since only one correction is calculated and used for all tagging algorithms and operating points commissioned up to date, an additional systematic uncertainty that covers the spread of the corrections for all these different operating points is added. All uncertainties are combined in quadrature. Only the most significant uncertainties are shown in the figure, namely the uncertainty that arises from the different correction for different operating points, and the uncertainty that arises from the limitations in the knowledge of the muon momentum spectrum in the center of mass of the decaying hadron. These uncertainties are estimated by reweighting that spectrum to match a measurement obtained in $e^+e^-$ scattering [41]. Due to the significant differences between that spectrum and the one found in PYTHIA, these variations are considered sufficient. All other uncertainties are combined and shown in

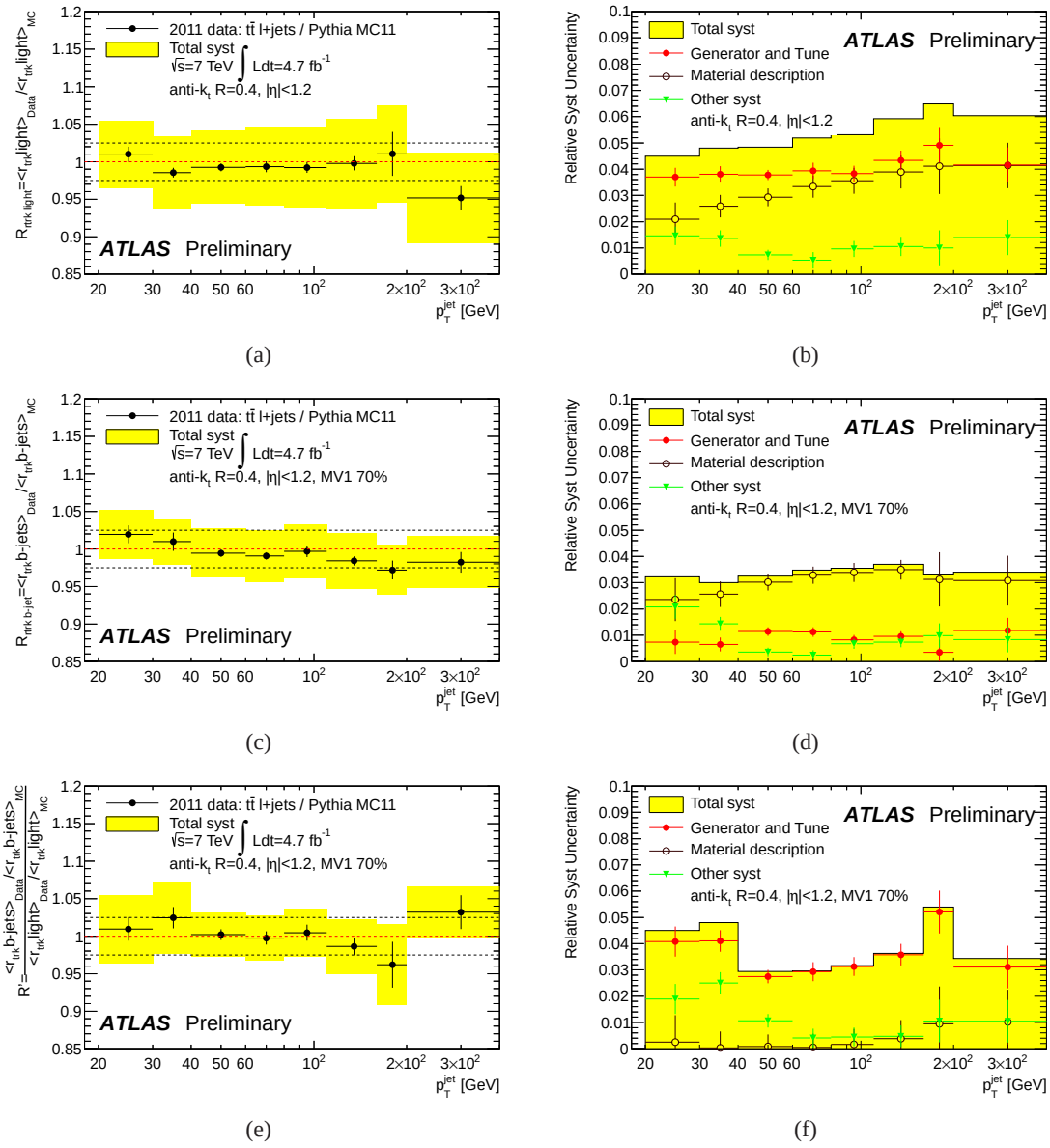


Figure 3: Ratio of the average $r_{\mathrm{trk}}$ in $t\bar{t}$ events in data and Monte Carlo simulation for light-jets (a) and tagged $b$-jets (c) and ratio of $R_{r_{\mathrm{trk}}}$ between the $b$-jet and the light-jet sample (e). The total systematic uncertainty is shown as a band, and the dotted lines correspond to 1 and the 2.5% deviation from 1. The contributions of the systematic uncertainties to the total uncertainty in the different measurements are shown in b, d, f. The contributions to the total systematic uncertainty due to the jet resolution, $b$-tagging calibration, background contamination and the modeling of the initial and final state radiation have been grouped under "Other systematics". Jets with $|\eta| < 1.2$ were used for these figures.

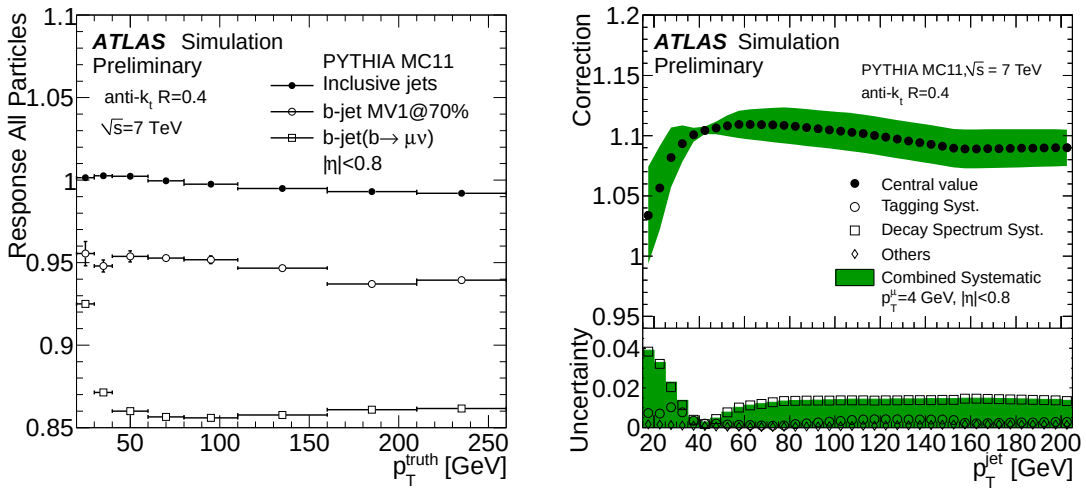


(a) (b)

Figure 4: a: Average jet response as a function of true transverse momentum of jets built using all stable particles, for a sample of inclusive jets (solid circles), a sample of $b$-jets tagged with the $MV1$ tagging algorithm (open circles) and a sample of semileptonically decaying $b$-jets with a reconstructed muon inside (open squares). b: Resulting semileptonic correction, as a function of calorimeter jet $p_{\mathrm{T}}$, used to transform the $p_{\mathrm{T}}$ of a jet in the semileptonic sample to the $p_{\mathrm{T}}$ of a jet in an inclusive sample of $b$-jets. Associated systematic uncertainties are shown around the central value, and the combined uncertainty is shown as a colored band.

the figure under the same curve.

The uncertainty is about 1.5% for most $p_{\mathrm{T}}$ values in the central region, except at low $p_{\mathrm{T}}$ where it increases to about 4%. The behavior is similar at larger $\eta$, except in the most forward bin ($2.1 < |\eta| < 2.5$), where variations across tagging operating points cause the uncertainty to increase to about 2%.

## 8 Semileptonic neutrino energy validation using dijet balance

The modeling of the energy carried by the neutrino in the inclusive $b$-jet sample and in the semileptonic $b$-jet sample can be validated using the $p_{\mathrm{T}}$ balance of a dijet system. The same technique has been used in Ref. [4] to validate the variation of the calorimeter response as a function of different jet properties. The response in data is calculated using the asymmetry in the jet $p_{\mathrm{T}}$ of the two jets in the dijet system. The two jets are required to be $b$-tagged, and the probe jet is required to have a selected reconstructed muon within $\Delta R < 0.4$. The relative response, calculated from the asymmetry, is sensitive to the energy carried by the neutrino, but also to the response differences between the $b$-tagged and semileptonic $b$-jet samples. These differences, however, are well modeled in the Monte Carlo simulation as shown in Section 6.2.

Figure 5 shows the relative response of semileptonic $b$-jets with respect to inclusive $b$-jets obtained in data and Monte Carlo simulation using dijet balance. The presence of neutrinos in the $b$-jet decay causes the estimated relative response to be below 1. The uncertainty band around the data represents systematic uncertainties in the imbalance. These are calculated through variations in the soft radiation cut in the selection (i.e. the $p_{\mathrm{T}}$ used for the veto on the third leading jet) as in Ref. [42]. An additional contribution to the uncertainty is added to the first $p_{\mathrm{T}}$ bin to account for differences between data and

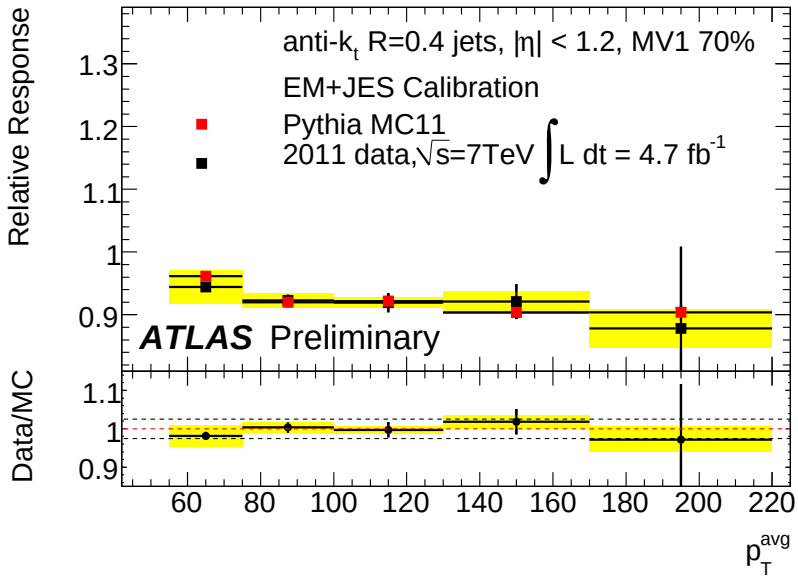


Figure 5: Relative response of the semileptonic sample with respect to the inclusive *b*-jet sample as calculated from the dijet $p_{\mathrm{T}}$ asymmetry. The uncertainty band around the data denotes systematic uncertainties in the asymmetry measurement.

Monte Carlo simulation in the turn-on of the efficiency curve for the jet-muon trigger used in this analysis. Agreement is found between data and Monte Carlo simulation, validating the description of this process that was exploited to develop the semileptonic correction presented in Section 7.

## 9 Conclusions

The uncertainty on the jet energy measurement has been studied for light jets as well as inclusive and semileptonic *b*-jets. In the inclusive QCD jet sample the jet energy scale has been probed using tracks associated with jets over a wide range of jet $p_{\mathrm{T}}$. Comparisons between data and Monte Carlo simulation show agreement within systematic uncertainties of approximately 3% with weak dependence on the transverse momentum of the jets. The *b*-jet energy scale has also been probed using tracks associated with *b*-tagged jets in the data. The results in the $t\bar{t} \rightarrow l$+jets and inclusive jet samples suggest that the jet energy scale of *b*-jets is well described in the Monte Carlo simulation, within systematic uncertainties of about $(2-3)\%$.

In the Monte Carlo simulation, a correction for semileptonic jets decaying to muons that corrects the transverse momentum measurement to that in an inclusive sample of *b*-jets has been derived. The systematic uncertainties in this correction are derived using Monte Carlo simulation and are about 2%. The uncertainty in the jet energy measurement due to effects specific to *b*-jets has also been derived using Monte Carlo simulations. This uncertainty ranges from 1 to 3%.

The energy scale of semileptonic *b*-jets decaying to muons has been probed in the dijet sample in parallel with a study of the energy carried by the accompanying neutrino. The latter confirms the results found in the Monte Carlo simulation within systematic uncertainties of about 3%. The results in the data systematically demonstrate a lower calorimeter response than in the Monte Carlo simulation, reaching about 4% at the lowest $p_{\mathrm{T}}$ probed (about 60 GeV), which is not fully covered by the systematic uncertainties.

## References


[1] ATLAS Collaboration, *Measurement of the top quark mass with the template method in the $t\bar{t} \to$ lepton + jets channel using ATLAS data*, Eur. Phys. J. **C72** (2012) 2046, arXiv:1203.5755 [hep-ex].

[2] ATLAS Collaboration, *Measuring the b-tag efficiency in a sample of jets containing muons with 5 $fb^{-1}$ of data from the ATLAS detector*, https://cdsweb.cern.ch/record/1435197, March, 2012. ATLAS-CONF-2012-043.

[3] ATLAS Collaboration, *Calibrating the b-tag efficiency and mistag rate in 35 $pb^{-1}$ of data with the ATLAS detector*, https://cdsweb.cern.ch/record/1356198, June, 2011. ATLAS-CONF-2011-089.

[4] ATLAS Collaboration, *Jet energy measurement with the ATLAS detector in proton-proton collisions at sqrt(s) = 7 TeV*, Submitted to EPJ (2011) , arXiv:1112.6426 [hep-ex].

[5] ATLAS Collaboration, *The ATLAS experiment at the CERN Large Hadron Collider*, JINST **3** (2008) S08003.

[6] M. Cacciari, G. P. Salam, and G. Soyez, *The anti-$k_t$ jet clustering algorithm*, JHEP **04** (2008) 063, arXiv:0802.1189 [hep-ph].

[7] ATLAS Collaboration, *Expected performance of the ATLAS experiment - detector, trigger and physics*, tech. rep., CERN, Geneva, September, 2009. arXiv:0901.0512 [hep-ex]. CERN-OPEN-2008-020.

[8] E. Abat et al., *Combined performance studies for electrons at the 2004 ATLAS combined test-beam*, JINST **5** (2010) P11006.

[9] M. Aharrouche et al., *Measurement of the response of the ATLAS liquid argon barrel calorimeter to electrons at the 2004 combined test-beam*, Nucl. Instrum. Meth. **A 614** (2010) 400–432.

[10] J. Colas et al., *Response uniformity of the ATLAS liquid argon electromagnetic calorimeter*, Nucl. Instrum. Meth. **A 582** (2007) 429–455, arXiv:0709.1094 [physics.ins-det].

[11] M. Aharrouche et al., *Energy linearity and resolution of the ATLAS electromagnetic barrel calorimeter in an electron test-beam*, Nucl. Instrum. Meth. **A 568** (2006) 601–623.

[12] P. Adragna et al., *Testbeam studies of production modules of the ATLAS Tile calorimeter*, Nucl. Instrum. Meth. **A 606** (2009) 362–394.

[13] J. Pinfold et al., *Performance of the ATLAS liquid argon endcap calorimeter in the pseudorapidity region* $2.5 < |\eta| < 4.0$ *in beam tests*, Nucl. Instrum. Meth. **A 593** (2008) 324–342.

[14] C. Cojocaru et al., *Hadronic calibration of the ATLAS liquid argon end-cap calorimeter in the pseudorapidity region* $1.6 < |\eta| < 1.8$ *in beam tests*, Nucl. Instrum. Meth. **A 531** (2004) 481–514.

[15] M. Aharrouche et al., *Study of the response of ATLAS electromagnetic liquid argon calorimeters to muons*, Nucl. Instrum. Meth. **A 606** (2009) 419–431.

[16] ATLAS Collaboration, *Electron performance measurements with the ATLAS detector using the 2010 LHC proton-proton collision data*, Eur. Phys. J. **C 72** (2012) 1909, arXiv:1110.3174 [hep-ex].

[17] ATLAS Collaboration, *Commissioning of the ATLAS high-performance b-tagging algorithms in the 7 TeV collision data*, http://cdsweb.cern.ch/record/1369219, July, 2011. ATLAS-CONF-2011-102.

[18] ATLAS Collaboration, *Measurement of the flavour composition of dijet events in pp collisions at $\sqrt{s}$ = 7 TeV with the ATLAS detector*, https://cdsweb.cern.ch/record/1460393, July, 2012. ATLAS-CONF-2012-081.

[19] ATLAS Collaboration, *Performance of missing transverse momentum reconstruction in proton-proton collisions at 7 TeV with ATLAS*, Eur. Phys. J. **C 72** (2012) 1844, arXiv:1108.5602 [hep-ex].

[20] T. Sjostrand, S. Mrenna, and P. Z. Skands, *PYTHIA 6.4 physics and manual*, JHEP **0605** (2006) 026, arXiv:0603175 [hep-ph].

[21] ATLAS Collaboration, *ATLAS tunes for Pythia6 and Pythia8 for MC11*, Tech. Rep. ATLAS-PHYS-PUB-2011-009, July, 2011.

[22] J. Pumplin et al., *New generation of parton distributions with uncertainties from global QCD analysis*, JHEP **07** (2002) 012, arXiv:0201195 [hep-ph].

[23] T. Sjostrand, S. Mrenna, and P. Z. Skands, *A Brief Introduction to PYTHIA 8.1*, Comput. Phys. Commun. **178** (2008) 852–867, arXiv:0710.3820 [hep-ph].

[24] ATLAS Collaboration, *The ATLAS simulation infrastructure*, Eur. Phys. J. **C 70** (2010) 823–874, arXiv:1005.4568 [physics.ins-det].

[25] A. Sherstnev and R. S. Thorne, *Parton distributions for LO generators*, Eur. Phys. J. **C 55** (2008) 553–575, arXiv:0711.2473 [hep-ph].

[26] M. Bahr et al., *Herwig++ physics and manual*, Eur. Phys. J. **C 58** (2008) 639–707, arXiv:0803.0883 [hep-ph].

[27] P. Z. Skands, *The Perugia Tunes*, arXiv:0905.3418 [hep-ph].

[28] A. Buckley, H. Hoeth, H. Lacker, H. Schulz, and J. E. von Seggern, *Systematic event generator tuning for the LHC*, Eur. Phys. J. **C 65** (2010) 331–357, arXiv:0907.2973 [hep-ph].

[29] M. Bowler, *$e^+$ $e^-$ Production of Heavy Quarks in the String Model*, Z. Phys. **C 11** (1981) 169.

[30] S. Frixione and B.R. Webber, *Matching NLO QCD computations and parton shower simulations*, JHEP **0206** (2002) 029, hep-ph/0204244.

[31] H.-L. Lai et al., *New parton distributions for collider physics*, Phys.Rev. **D82** (2010) 074024, arXiv:1007.2241 [hep-ph].

[32] G. Corcella et al., *HERWIG 6: An Event generator for hadron emission reactions with interfering gluons (including supersymmetric processes)*, JHEP **0101** (2001) 010, hep-ph/0011363.

[33] J. M. Butterworth, J. R. Forshaw, and M. H. Seymour, *Multiparton interactions in photoproduction at HERA*, Z. Phys. **C72** (1996) 637–646, arXiv:hep-ph/9601371.

[34] ATLAS Collaboration, *ATLAS tunes for Pythia6 and Pythia8 for MC11*, Tech. Rep. ATL-PHYS-PUB-2011-008, May, 2011.

[35] S. Frixione, P. Nason and C. Oleari, *Matching NLO QCD computations with Parton Shower simulations: the POWHEG method*, JHEP **0711** (2007) 070, arXiv:0709.2092[hep-ph].

[36] B.P. Kersevan and E. Richter-Wąs, *The Monte Carlo event generator AcerMC version 2.0 with interfaces to PYTHIA 6.2 and HERWIG 6.5*, (2004) , hep-ph/0405247.

[37] A. Sherstnev and R. Thorne, *Different PDF approximations useful for LO Monte Carlo generators*, arXiv:0807.2132 [hep-ph].

[38] ATLAS Collaboration, *Measurement of ttbar production with a veto on additional central jet activity in pp collisions at $\sqrt{s}$ = 7 TeV using the ATLAS detector*, Eur. Phys. J. **C72** (2012) 2043, arXiv:1203.5015 [hep-ex].

[39] ATLAS Collaboration, *Jet energy scale and its systematic uncertainty in proton-proton collisions at $\sqrt{s}$=7 TeV with ATLAS 2011 data*, January, 2013. ATLAS-CONF-2013-004.

[40] ATLAS Collaboration, *Charged-particle multiplicities in p-p interactions measured with the ATLAS detector at the LHC*, New J.Phys. **13** (2011) 053033, arXiv:1012.5104 [hep-ex].

[41] DELPHI Collaboration, *Determination of heavy quark non-perturbative parameters from spectral moments in semileptonic B decays*, Eur. Phys. J. **C 45** (2006) 35–59.

[42] ATLAS Collaboration, *In situ jet pseudorapidity intercalibration of the ATLAS detector using dijet events in sqrts=7 TeV proton-proton 2011 data*, https://cdsweb.cern.ch/record/1474490, August, 2012. ATLAS-CONF-2012-124.

# A Additional plots

## A.1 Additional plots for the inclusive analysis

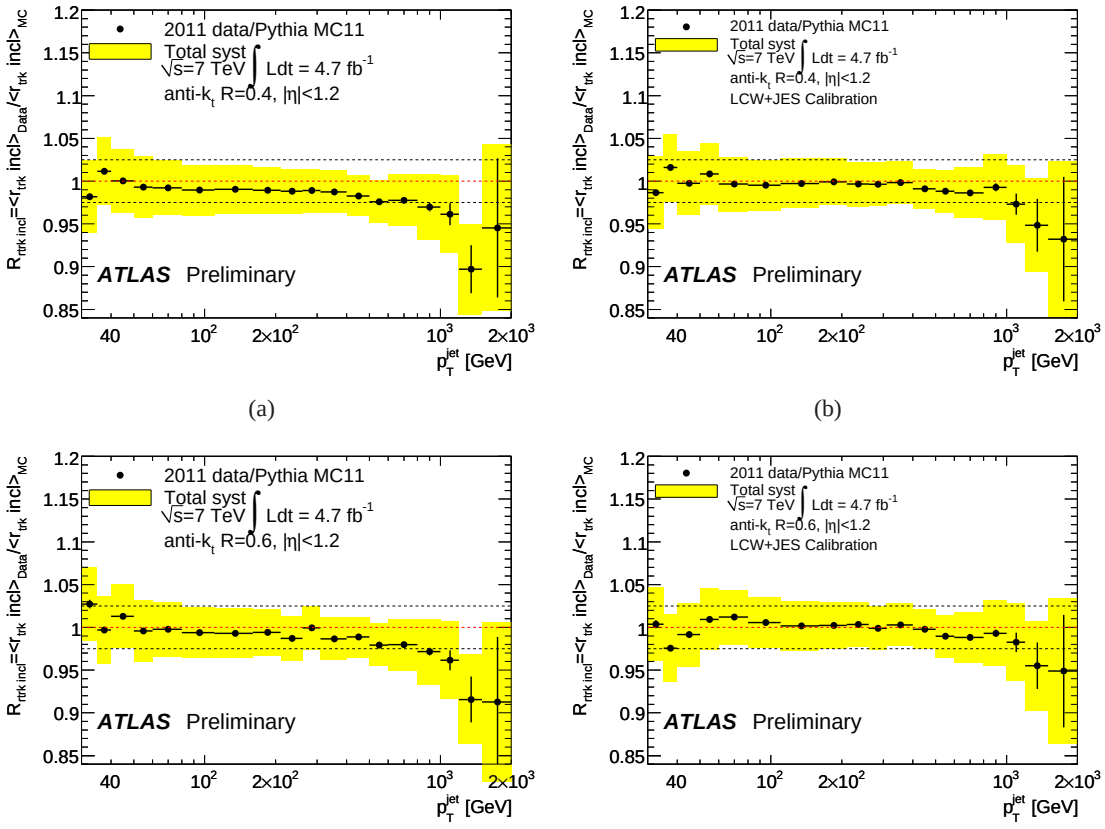


Figure 6: Ratio of the average $r_{\mathrm{trk}}$ in data and Monte Carlo simulation in the inclusive jet sample for anti-$k_t$ jets calibrated with the EM+JES (a, c) and LCW+JES (b, d) calibrations, for jets with $|\eta| < 1.2$ built with resolution parameter $R = 0.4$ (a, b) and $R = 0.6$ (c, d).

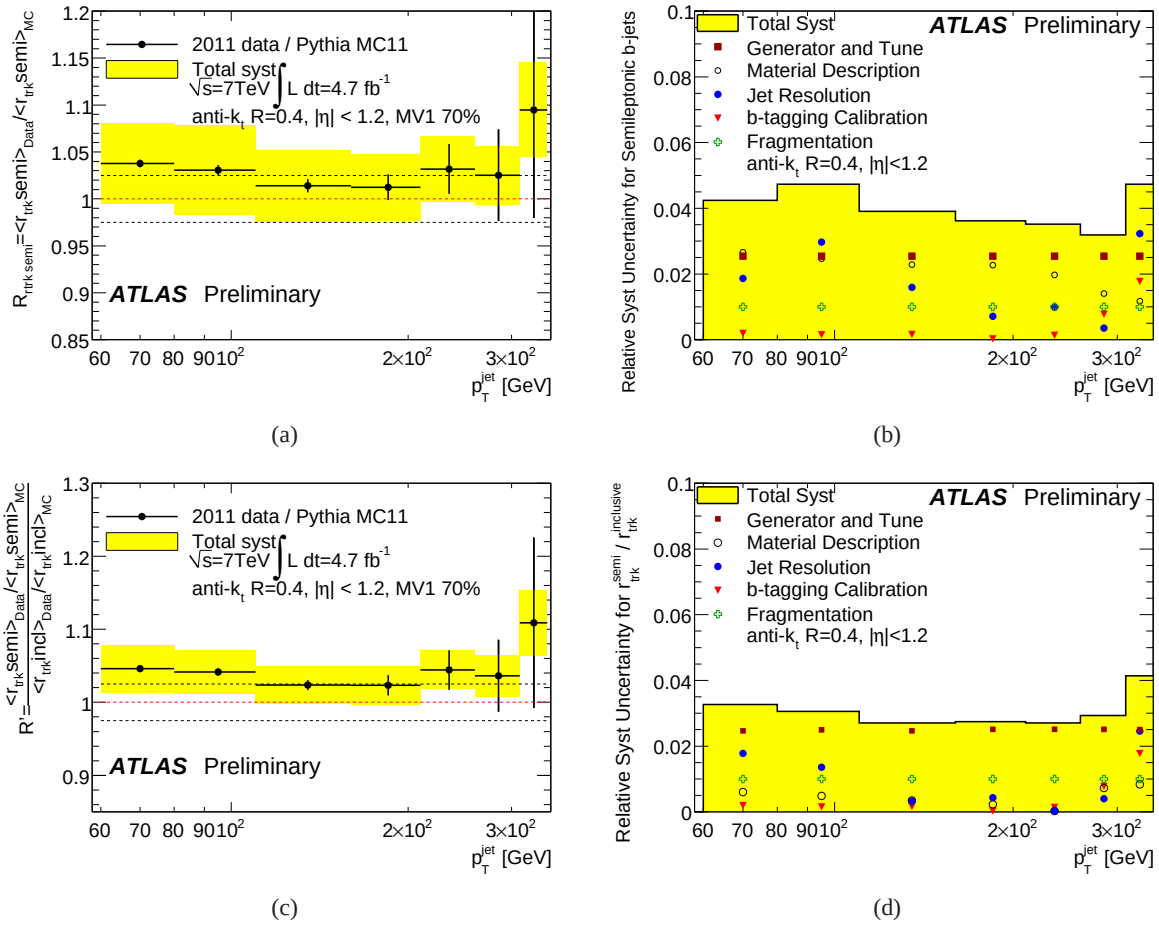


Figure 7: Ratio of the average $r_{\mathrm{trk}}$ in data and Monte Carlo simulation in the semileptonic $b$-jet sample made of tagged jets with $|\eta| < 1.2$ and a muon inside (a). The ratio of $R_{r_{\mathrm{trk}}}$ between this sample and the inclusive jet sample is also shown (c), as well as the different components of the systematic uncertainties for these two measurements (b,d). Jets are built using the anti-$k_t$ algorithm with resolution parameter $R = 0.4$, and calibrated with the EM+JES calibration.

## A.2 Additional plots for the top-quark pair analysis

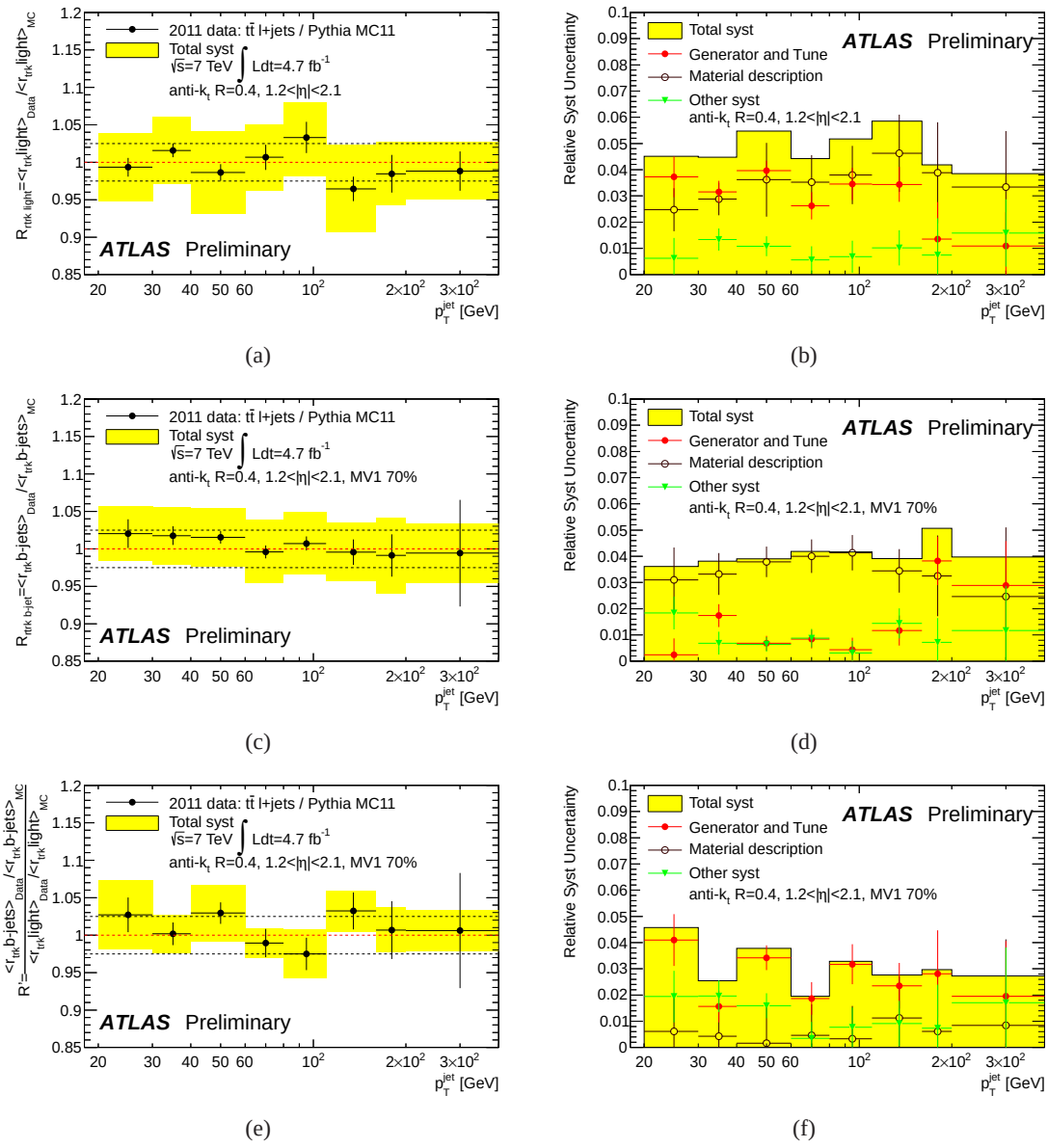


Figure 8: Ratio of the average $r_{\mathrm{trk}}$ in $t\bar{t}$ events in data and Monte Carlo simulation for light-jets (a) and tagged $b$-jets (c) and ratio of $R_{r_{\mathrm{trk}}}$ between the $b$-jet and the light-jet sample (e). The total systematic uncertainty is shown as a band, and the dotted lines correspond to 1 and the 2.5% deviation from 1. The contributions of the systematic uncertainties to the total uncertainty in the different measurements are shown in b, d, f. The contributions to the total systematic uncertainty due to the jet resolution, $b$-tagging calibration, background contamination and the modeling of the initial and final state radiation have been grouped under "Other systematics". Jets with $1.2 < |\eta| < 2.5$ were used for these figures.

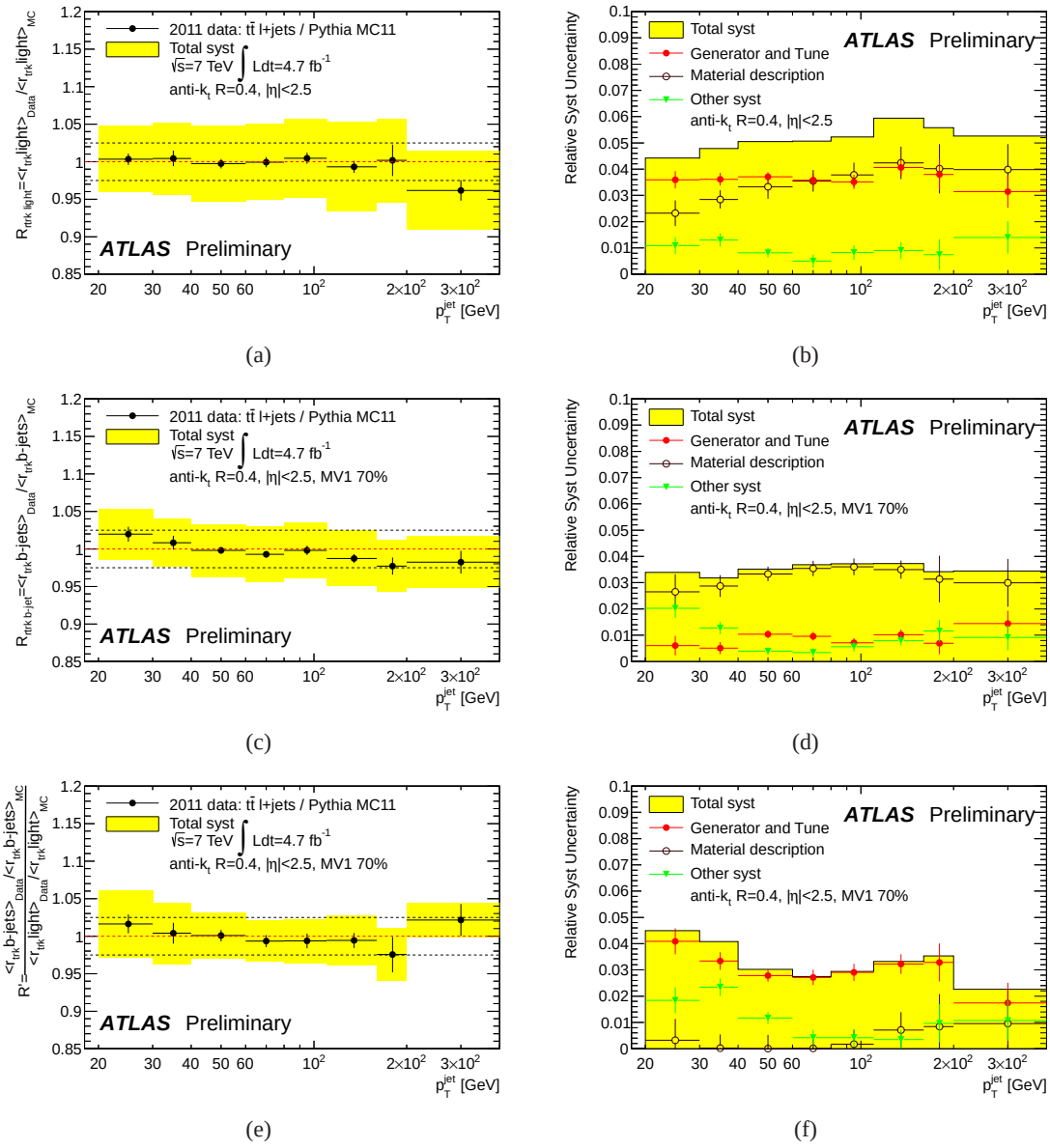


Figure 9: Ratio of the average $r_{\mathrm{trk}}$ in $t\bar{t}$ events in data and Monte Carlo simulation for light-jets (a) and tagged $b$-jets (c) and ratio of $R_{r_{\mathrm{trk}}}$ between the $b$-jet and the light-jet sample (e). The total systematic uncertainty is shown as a band, and the dotted lines correspond to 1 and the 2.5% deviation from 1. The contributions of the systematic uncertainties to the total uncertainty in the different measurements are shown in b, d, f. The contributions to the total systematic uncertainty due to the jet resolution, $b$-tagging calibration, background contamination and the modeling of the initial and final state radiation have been grouped under "Other systematics". Jets with $|\eta| < 2.5$ were used for these figures.

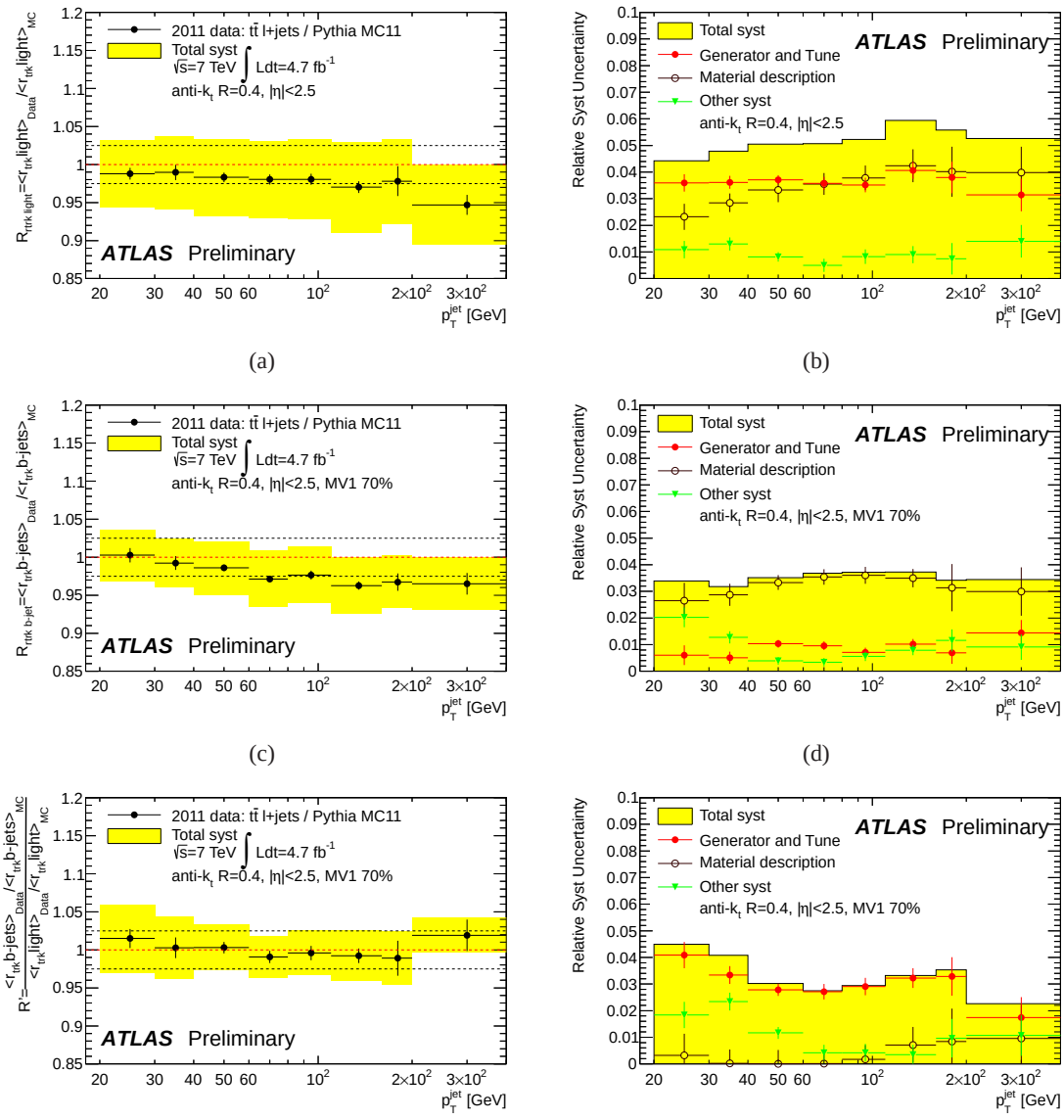


Figure 10: Same as Figure 9 but after the application of the jet energy scale correction derived using in-situ techniques [39] to the data.

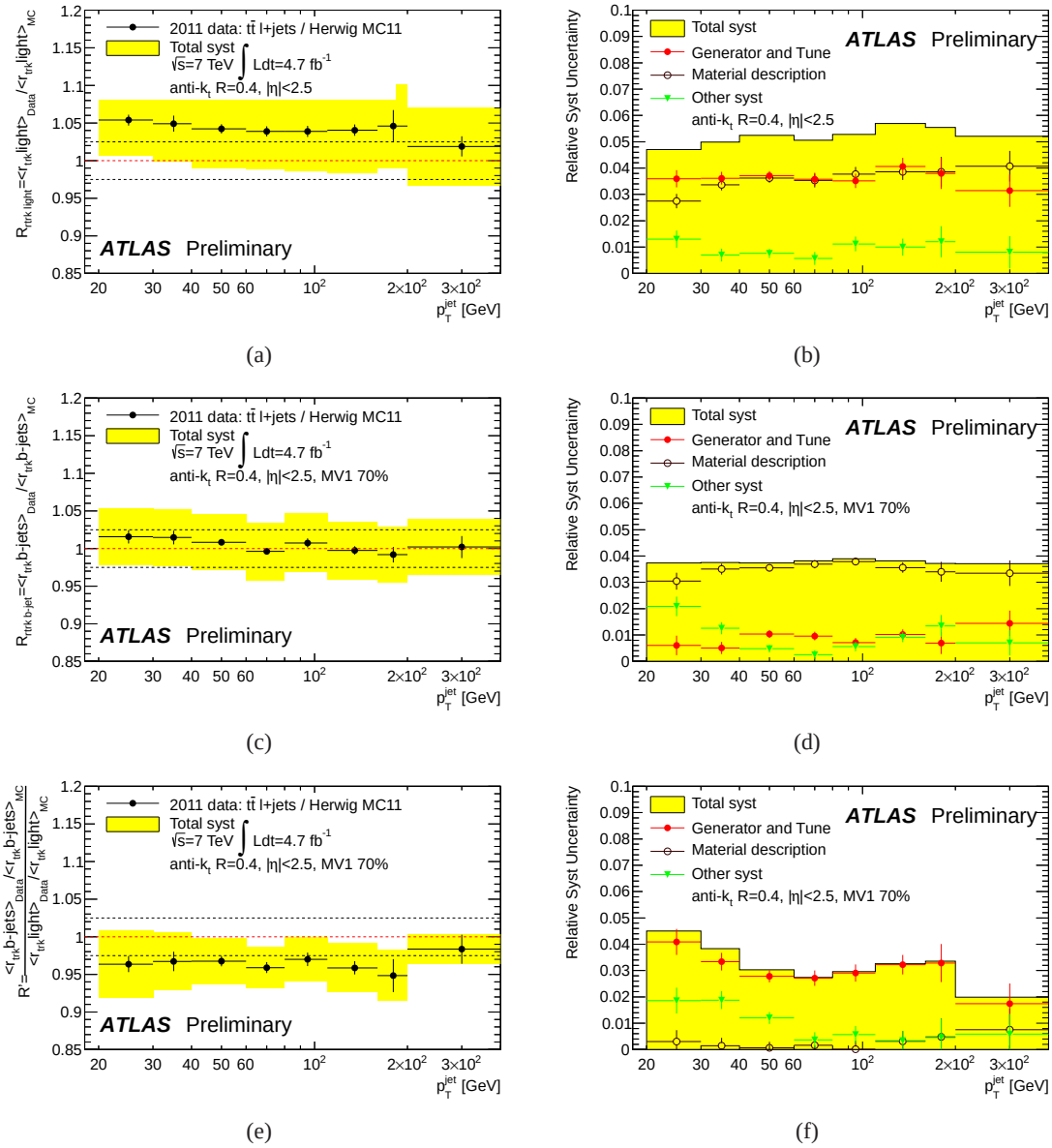


Figure 11: Same as Figure 9, but using MC@NLO+HERWIG+JIMMY simulated $t\bar{t}$ events for the comparison with data.

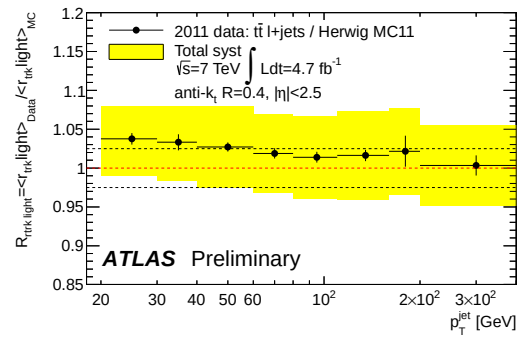


(a)

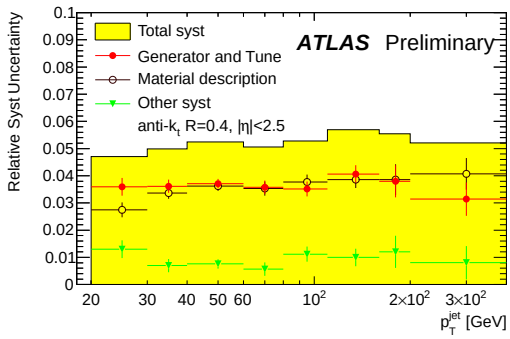


(b)

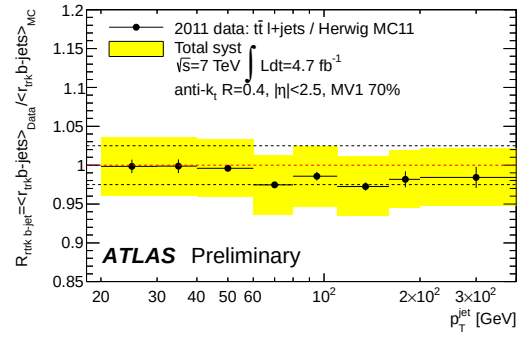


(c)

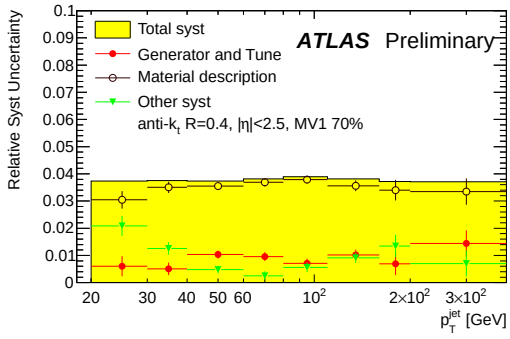


(d)

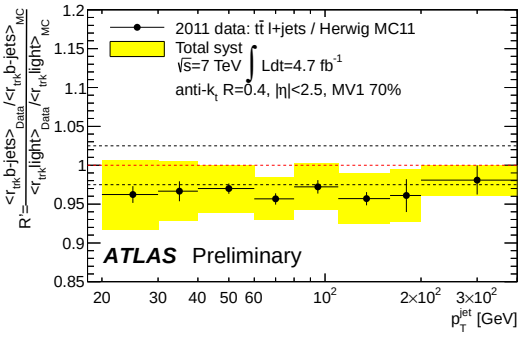


(e)

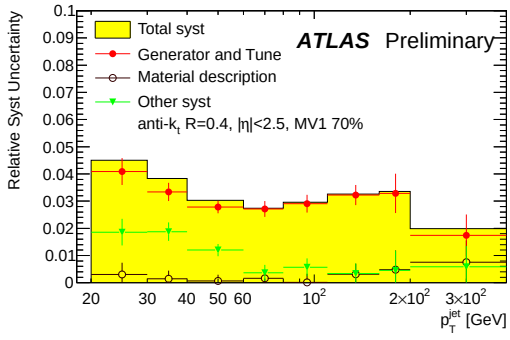


(f)

Figure 12: Same as Figure 11, but after the application of the jet energy scale correction derived using in-situ techniques [39] to the data.